Anal Bioanal Chem (2004) 378 : 1678–1692
DOI 10.1007/s00216-004-2526-0

PAPER IN FOREFRONT

Jonas O. Tegenfeldt · Christelle Prinz · Han Cao
Richard L. Huang · Robert H. Austin · Stephen Y. Chou
Edward C. Cox · James C. Sturm

Micro- and nanofluidics for DNA analysis

Received: 5 November 2003 / Revised: 23 January 2004 / Accepted: 27 January 2004 / Published online: 5 March 2004

Abstract Miniaturization to the micrometer and nanometer scale opens up the possibility to probe biology on a length scale where fundamental biological processes take place, such as the epigenetic and genetic control of single cells. To study single cells the necessary devices need to be integrated on a single chip; and, to access the relevant length scales, the devices need to be designed with feature sizes of a few nanometers up to several micrometers. We will give a few examples from the literature and from our own research in the field of miniaturized chip-based devices for DNA analysis, including dielectrophoresis for purification of DNA, artificial gel structures for rapid DNA separation, and nanofluidic channels for direct visualization of single DNA molecules.

Introduction

Many fundamental processes of biology, for example, information storage, transcription, translation, gene regulation, mitosis, and cell communication [1, 2, 3, 4], occur on the micrometer to nanometer scale. Using micro- and nanofabrication technology developed for the microelectronics industry, devices can readily be made on these length scales, thus enabling studies of single molecules and cells [5, 6] (Fig. 1).

The general benefits of miniaturization are of course the usual *quantitative* improvements [7]: less reagents, parallel analysis, faster operation, and more sensitive detection. More interesting are the new *qualitative* possibilities: (1) direct manipulation of relevant bio-entities such as proteins, nucleic acids, biomolecular complexes and organelles such as ribosomes and mitochondria, and whole cells; (2) high-resolution analysis using local light sources and detectors or local electrical detection; and (3) single-cell analysis by integration of several biochemical steps into a micro total analysis system (μTAS) on one single chip.

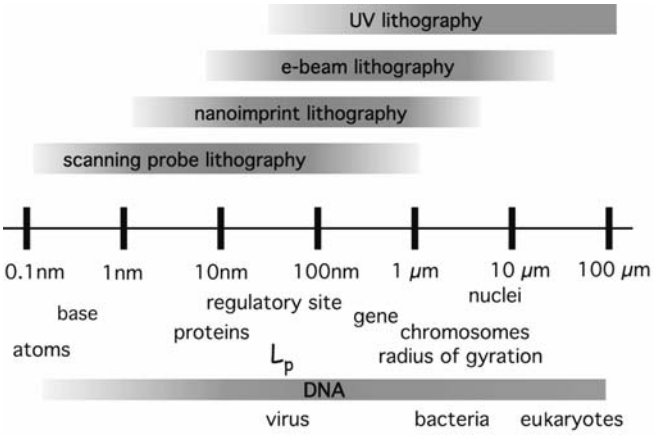

Fig. 1 The length scales of the fundamental building blocks of biology overlap with the length scales realizable using micro- and nanofabrication technology from the microelectronics industry. The persistence length (L_p) of DNA is given for standard physiological conditions. The gene size corresponds to the typical size of 1 kbp excluding any non-coding regions (introns). The chromosome size range corresponds to metaphase condensed chromosomes. The radius of gyration is indicated for DNA molecules ranging in size from 100 kbp to 100 Mbp

J. O. Tegenfeldt (✉) · E. C. Cox
Department of Molecular Biology, Princeton University, Princeton, NJ, USA
e-mail: jonas.tegenfeldt@ftf.lth.se

C. Prinz · R. H. Austin
Department of Physics, Princeton University, Princeton, NJ, USA

H. Cao · R. L. Huang · S. Y. Chou · J. C. Sturm
Department of Electrical Engineering, Princeton University, Princeton, NJ, USA

Present address:
J. O. Tegenfeldt
The Division of Solid State Physics, Lund University, Lund, Sweden

Present address:
C. Prinz
The Division of Solid State Physics, Lund University, Lund, Sweden

Present address:
H. Cao
BioNanomatrix, Blawenburg, NJ, USA

Conventional bioanalytical technology relies almost exclusively on the measurements of cell populations. For example, for transcription profiling, mRNA is extracted from a collection of cells (typically 10^7 cells) under specific conditions. cDNA is prepared from the extracted mRNA using reverse transcriptase and is analyzed using DNA microarrays [8]. The presence of cDNA corresponds to the activity of the corresponding gene. The experiment is repeated for various conditions, and the structure of the underlying regulatory network can be deduced by correlating the transcriptional profiles with the corresponding experimental conditions. Although vastly popular and successful, there are shortcomings: (1) the measurements give information of the population average, and the existence of subpopulations cannot be discerned; (2) the measured transcriptional profile of the genes associated with the cell cycle will consist of an average over all cell cycles unless the cells are synchronized. This can be done for certain cells but not for all. Single-cell measurements have the potential to complement population-based methods by circumventing these shortcomings.

However, it is difficult to handle and manipulate single cells routinely using conventional technology, since very small volumes are involved: for example, the total volume of a typical prokaryotic cell such as *E. coli* is on the order of 10 fL, and for a typical eukaryotic cell 10 pL. Furthermore, the genome of even simple organisms is several million base pairs long (equivalent to a single molecule 1 mm in length), and much longer for more complex organisms. These DNA molecules shear if pipetted. On the other hand, in the low-Reynolds-number environment of a microfluidic chip, genomic material can be transported easily without shearing. Therefore, to routinely handle single cells and their contents independently, all steps from cell sorting to analysis of the molecular cell contents including DNA analysis must be realized on a single microfabricated platform.

In our work the ultimate goal is to harvest the following information from the DNA molecules extracted from a single cell: (1) binding of control factors and other modifications along the DNA; (2) genetic contents; (3) length distribution of DNA fragments. The idea is then to correlate the data with the state of the individual cell to learn more about the complex, underlying networks that control it.

Control factors

A large range of proteins bind to DNA [9] and are involved in DNA replication, DNA folding [10], and gene control. One very important group of control proteins are the transcription factors, which bind adjacent to specific genes along the DNA [3, 4] controlling the activity of the corresponding genes. Another level of control is modification of the DNA itself. Methylation of the base cytosine may control whether genes are switched on or off [11, 12] and is important for genomic imprinting [13]. This type of modification, in addition to histone acetylation, is one of the most important epigenetic modifications of DNA, that is, modifications to the genome that do not involve changes in the sequence. With nanotechnology there is a potential to access the DNA on the length scale of the control factors and modifications, and thereby directly read out the epigenetic factors that control the expression of the genes along the DNA.

Genetic contents

Genetic variations are interesting because of their medical implications: they are the underlying factor for many diseases, and they may determine susceptibility to certain medications. Single nucleotide polymorphisms (SNPs), that is, variations in single bases, are very important in this context [14]. To map SNPs or linked groups of SNPs [15, 16], various techniques have been developed [17]. Perhaps the most straightforward approach is based on hybridization of fluorescent sequence-specific probes and detection in DNA microarrays. Another possibility is to use restriction enzymes that cut specific sequences [18]. By measuring the length distribution of a DNA sample after cutting with a specific restriction enzyme, variations that are associated with the cutting sites are easily located by the absence or presence of the corresponding lengths. Nanotechnology can be used to create devices for single-molecule analysis of DNA and for direct visualization of cut DNA or of fluorescent sequence-specific probes bound along the DNA.

Length distribution

Gel-based techniques have been the workhorse for molecular biology during the past decades mainly for sequencing of DNA, but also for characterization of, for example, BAC and PAC libraries. There are, however, drawbacks with present approaches. Standard gel-based techniques with constant applied electric fields limit the separation to short DNA (c.a. <40 kbp). The duration of pulsed-field gel electrophoresis for separation of long, chromosome-sized DNA can be many days (10 days for separation of 9-Mbp DNA [19]). Miniaturization and the fabrication of artificial gels speed up the separation of DNA for length measurements [20, 21], and using nanofluidic channels, DNA may be stretched and visualized directly for the rapid determination of length distributions.

In this review we will discuss requirements and challenges in DNA analysis using nano- and microfabricated devices. We will give an overview of some of the available fabrication techniques, discuss some general considerations, and then continue with examples of devices made for analysis of DNA for the ultimate goal of single-cell studies on a chip.

Fabrication

There exists a wide range of micro- and nanofabrication techniques, which directly access the relevant length

scales from nanometers to millimeters as shown in Fig. 1. More specific requirements are discussed in the "Design considerations" section later.

Microfabrication techniques [22, 23] are being pushed every year to higher resolution and complexity [24]. As of 2003, standard memory devices are made using UV lithography at a wavelength of 193 nm and with a 90-nm linewidth on 300-mm wafers [25]. Soft X-ray or extreme-UV (EUV) lithography [26, 27] is being developed by several consortia all over the globe to push the resolution to smaller length scales. The present goal is to make features on a 45-nm scale using light with 13.4-nm wavelength. EUV lithography is technologically very challenging and far from being realized for the commercial market. Instead, for prototyping, lithography technologies based on focused beams are more readily available, such as electron beam lithography (EBL) and focused ion beam (FIB) lithography. In EBL, a focused beam of electrons is scanned over a resist, such as poly(methyl methacrylate) (PMMA), breaking bonds. The exposed areas are then selectively dissolved in a carefully selected organic solvent. EBL is typically capable of writing features on a 10-nm scale. In FIB lithography, a focused ion beam (generally Ga ions) is scanned over a sample surface, sputtering away material on a 10-nm scale. The exposure time at each point determines the sputtering depth so that three-dimensional structures can be made. To increase selectivity and material-removal rates, reactive gases, such as XeF_2, can be added locally. Gases can also be added for deposition of materials such as platinum or SiO_x, with a resolution of about 100 nm. FIB lithography is therefore an extremely versatile technique for making arbitrary micro- and nanostructures with essentially no required pre- or postprocessing. For the ultimate resolution, scanning probe techniques must be used, such as atomic force microscopy (AFM) [28] and scanning tunneling microscopy (STM); the latter is capable of positioning single atoms on a surface [29]. The focused beam technologies, and especially the scanning probe technologies, are all serial techniques with very low throughput. In nanofluidics experiments it is important to have access to large numbers of devices to be able to perform repeated well-controlled experiments, since they are notoriously sensitive to contamination of the surfaces facing the nanochannels, and due to the difficulty of cleaning the channels. There is therefore a need for high-throughput, parallel lithography techniques. Nanoimprinting lithography (NIL) [30, 31, 32] is a very promising candidate for large-scale nanofabrication. It is based on a simple idea. First, a mold is made using, for example, EBL, FIB, or optical lithography. To make large areas of uniform nanoscale features, interference lithography [33, 34, 35] is a useful technique. In this way it is possible to create arrays of nanoscale lines or pillars over 100-mm wafers. Once the mold is made, it is pressed into a thermoplastic polymer spun on a wafer, leaving an imprint in the plastic. The resulting pattern is then transferred to the wafer using, for example, lift-off or reactive ion etching [23]. The process transfers the pattern from the mold into the wafer with nanometer fidelity and takes a few minutes. This can be repeated up to 1,000 times depending on the surface treatments and polymers used.

Self-assembly works on the nanoscale and can be used to define large areas with nanoscale features [36, 37, 38, 39, 40, 41]. By defining seeding structures on the underlying substrate, the nature and the orientation of the self-assembled film can be controlled [42]. In colloidal crystallization [42, 43] microspheres are allowed to organize in close-packed structures on surfaces and in microchannels (Fig. 2). Close-packed beads create a three-dimensional array with holes with a diameter of approximately 15% the size of the beads. For crystals based on beads with a diameter of 100 nm, we thus have pores with size approximately 15 nm, which is comparable to the typical pore sizes of standard polyacrylamide gels (1–10 nm) and less than the pore sizes in agarose gels (100–1,000 nm).

Sealing of etched structures to create channels is a major challenge. The sealing structure must be reliable and not intrude into the channel.

For rapid prototyping, polydimethylsiloxane-covered cover glasses are good for sealing devices. Polydimethylsiloxane (PDMS) is spun onto a cover slip to a thickness of several microns and allowed to cure. The PDMS is then brought into contact with the chip containing the trenches.

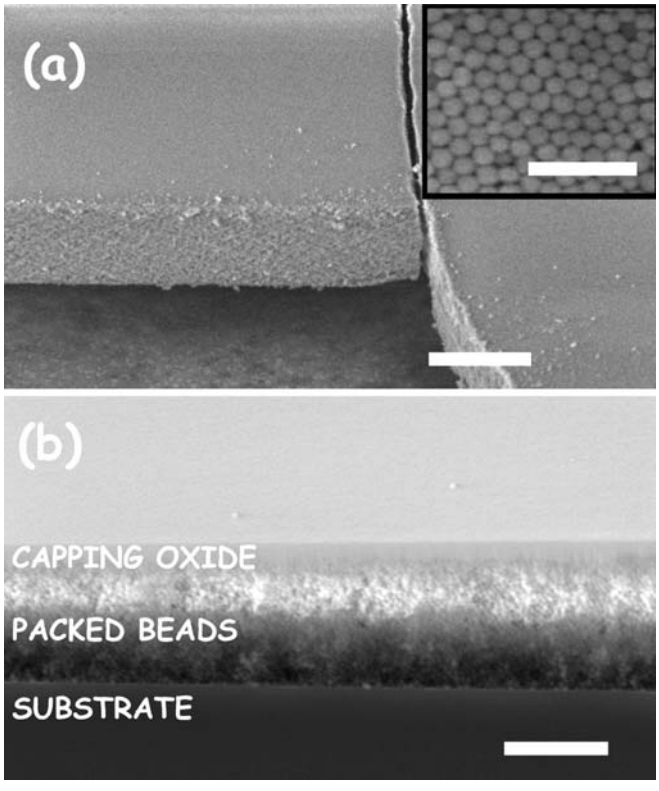

Fig. 2 **a** A several-microns-thick layer of hexagonally close-packed beads is the result of spontaneous ordering of silica beads after drying a suspension on a flat surface. The *scale bar* is 10 µm. The *insert* shows a magnified part of the surface. The *scale bar* of the insert is 500 nm. **b** One way of creating a microfluidic channel filled with close-packed beads is to deposit a thin film of SiO_x on top. The *scale bar* is 2 µm (JO Tegenfeldt, unpublished work. At Princeton University WW Reisner continues the work)

Oxygen plasma pretreatment of selected areas of the PDMS can be used to make it hydrophilic although it may degrade the PDMS and induce sticking. Another approach is to treat the channels with triblock copolymers, which prevent protein adhesion as well as rendering the surface hydrophilic. The result is reversibly sealed channels that can easily be opened up for cleaning. The disadvantage is that the seal can fail during an experiment especially if the channels occupy a significant fraction of the total area of the chip. Another disadvantage is that the PDMS is soft and can sag into shallow channels, resulting in defects and sticking of the molecules moving in the channels.

Wafer bonding [44] is a very reliable way to seal trenches in order to create channels. Anodic bonding of Pyrex glass on silicon is commonly used, but since it relies on electrically conducting materials, problems may occur in cases where high electric field strengths are required such as in electrokinetic movement of samples. Instead silica–silica bonding is preferred. This also makes the devices especially useful for single-molecule applications because of the low endogenous fluorescence of fused silica.

Instead of attaching an additional wafer on top of any etched structures, direct sealing can be employed to create channels. One example is based on nonuniform deposition during sputtering deposition. In the deposition chamber the material is deposited at a wide distribution of angles. The sidewalls of an etched trench will block any material coming in at a large angle from the normal of the wafer. The result is a nonuniform deposition rate with a high rate at the top of the sidewalls of the trenches and a low rate at the bottom [45]. The process results in narrowed and eventually sealed trenches (Fig. 3). In this way we were able to make sealed 10-nm-diameter channels starting from 55-nm-diameter trenches [46].

Using sacrificial materials is another approach to directly create sealed channels. Compared to the nonuniform deposition described above [45, 46], it allows very thin walls of the channels, which may be an advantage for integration of microelectronics components, such as light sources and detectors. The basic idea is simple. The sacrificial

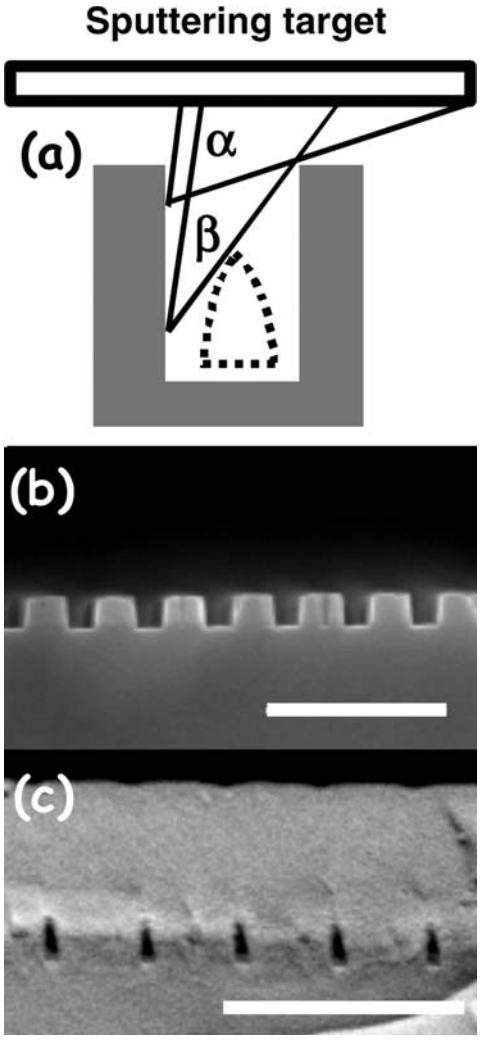

Fig. 3a–c Channels made by deposition of SiO_x from a large sputtering target resulting in narrowed and eventually sealed channels. **a** Due to shadowing by the edges, the bottom part of the trench is subjected to deposition from a smaller part of the target and thus a smaller deposition rate. Conversely, the edges are subjected to a greater deposition rate. **b** The original channels before deposition were 65-nm wide. **c** After deposition the channels were narrowed down to 17 nm and sealed. The *scale bars* are all 500 nm (reproduced from ref. [46] with permission from the American Institute of Physics)

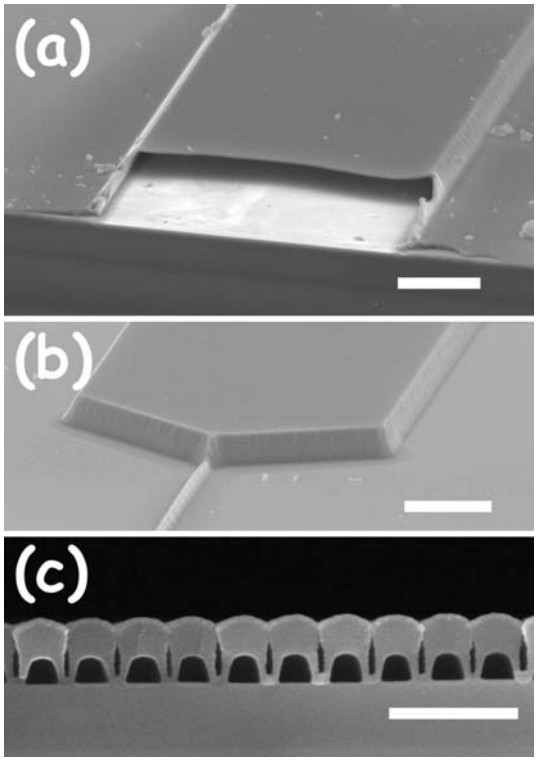

Fig. 4a–c Sealed channels made using sacrificial polymers and SiO_2 capping. **a** Large channels; the *scale bar* is 10 µm. **b** A small channel is combined with a large channel; the *scale bar* is 10 µm. **c** Small channels made with nanoimprinting lithography; the *scale bar* is 500 nm (adapted from ref. [51] with permission from IOP Publishing Limited)

polymer (e.g., polysilicon [47], polycarbonate [48, 49], or polynorbornene [50]) is deposited on a wafer forming a thin film. It is then patterned using standard lithographical techniques. A capping layer consisting of SiO_x or SiN_x is deposited on top. In the case of polysilicon, an etchant is used to remove the material. In the case of a sacrificial polymer the whole wafer is simply brought to an elevated temperature. The polymer disintegrates resulting in hollow channels. Using nanoimprinting lithography we were able to make 100-nm-wide channels in this way [51] (Fig. 4).

Instead of using processes from the microelectronics industry with materials such as silicon, oxides, and nitrides, soft lithography [52, 53, 54, 55], commonly based on silicone rubber, is suitable for simple, cheap, and rapid prototyping of sealed microfluidics systems including valves and pumps [56]. To increase the complexity of fluidic systems, the devices can be built in three dimensions realizing, for example, a fluidic multiplexer where dilution series can be prepared to find the optimum conditions for chemical reactions involving rare reagents [57]. An additional benefit of soft lithography is that temporary channels can be made for local chemical treatment of surfaces, which is useful for both patterning of biomolecules [58] and microfabrication [59].

Design considerations

The fundamental properties of fluidics on the micro- and nanoscale differ significantly from our daily experience. The flow is laminar and in the low-Reynolds-number regime, so that viscous forces dominate inertial forces [60, 61].

For a cylinder, the *surface-to-volume ratio* is inversely proportional to its diameter. This has two important implications: (1) as the diameter of a channel decreases it becomes increasingly difficult to move liquids using pressure gradients due to the increasing viscous drag of the walls. This makes it important to combine small channels for analysis with larger channels for bulk liquid transport. (2) Non-specific binding of reagents to surfaces is a problem that grows as the surface-to-volume ratio increases. It is thus very important to passivate and to tune the surface properties of all surfaces that come into contact with the sample solution.

Fluid and sample transport is a crucial issue in microfluidics and is mainly performed by applying pressure to a channel or electrokinetically by applying an electric field over the channel. One interesting variant of pressure-driven flow is to spin the device and utilize centrifugal forces [62]. Pressure-driven flow has in general a parabolic flow profile and requires very high pressures to achieve reasonable flow rates for nanoscale channels. Parabolic flow degrades separation assays. For nanoscale channels with diameters approaching the diffusion length of the sample, Taylor diffusion [63] may render the flow plug-like. Still, the required pressures make many designs impractical. To illustrate the problem, consider fluid flow in a cylindrical tube of radius R. With a pressure difference of ΔP between the ends of the tube, the velocity (v) of the fluid in the tube is given by [64] the equation $v = \frac{\Delta P R^2}{8\eta L}$. Consider typical values of ΔP=100 kPa (1 atm), standard buffer solution based on water (η=10^{-3} kg m^{-1} s^{-1}), and a channel length (L) of 100 µm. For a channel of diameter 1 µm we then have a velocity of 30 mm s^{-1}, whereas for a 100-nm-diameter channel we have a velocity of 300 µm s^{-1}, and in a 10-nm channel we would have a velocity of just 3 µm s^{-1}. We can clearly see that we need to design the device so that any necessary liquid transport is carried out in large channels, that the nanochannels are made as short as practical, and that any dead volumes are minimized. A *T-junction* arrangement (Fig. 5) addresses these concerns. Speed is gained by separating the fluid flows so that the analysis is carried out in the nanochannels and the bulk liquid transport in the larger microchannels. Any dead volume in the system is transported through the larger channels and avoids the nanochannels.

An alternative to pressure-driven flow is electrokinetic flow by electroendosmosis. Electroendosmosis is the movement of liquid in narrow capillaries with charged walls of diameter less than approximately 100 µm. Provided the walls are uniformly charged, electroendosmosis is a use-

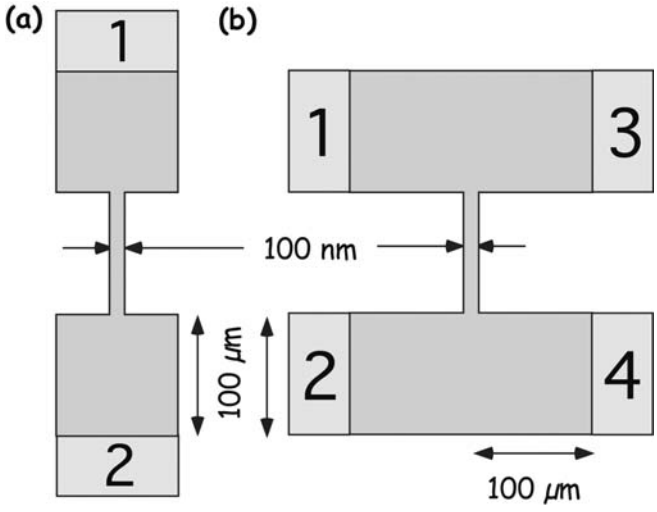

Fig. 5a, b Two microfluidic designs. The access holes are labeled *1–4*. Typical values for the dimensions of the channels are: cross sections 100 nm×100 nm and length 100 µm for the small channels and 1 µm×100 µm×200 µm (depth×width×length) for the larger ones. The submicron channels are not drawn to scale. Assume standard conditions with an applied pressure difference of 100 kPa and water at 20°C so that the viscosity η=10^{-3} kg m^{-1} s^{-1}. The cycle time is defined as the time it takes to introduce a new liquid and pump it through the nanochannel. For a simple two-reservoir device (**a**), all liquid in the large-channel area must be pumped through the nanochannel until the next liquid sample can be introduced giving a cycle time of the order of an hour. In the double T-junction design (**b**), the liquid is first moved quickly in the microchannel into position close to the nanoscale channels by applying a pressure difference from *left* to *right* in the *upper channel* between *reservoirs 1* and *3*. Then the required amount is passed through the nanochannels by applying a pressure difference between the *upper reservoirs 1* and *3* on one side and *lower reservoirs 2* and *4* on the other. This gives us a cycle time of less than a second, which is more than three orders of magnitude faster

ful and widely used technique to pump liquid. The advantage is that the flow is independent of the radius of the channels and that the flow is plug-like, at least for channel diameters $\gg\Sigma$Debye length (1–10 nm under standard buffer conditions). The disadvantage is that the flow is strongly dependent on the surface charge distribution of the capillary walls, which is easily affected by, for example, adsorption of contaminants, making the flow sometimes difficult to control. For DNA movement, when there is no requirement to move the fluid, electrophoresis is probably the best alternative. In that case electroendosmosis can be suppressed [65, 66, 67, 68] by increasing the viscosity locally at the walls of the channels or by decreasing the zeta potential. To this end, we have had good experience adding POP-6 (Applied Biosystems, Foster City, CA), a linear polyacrylamide, to our running buffers at a concentration of 0.1%.

Surface modification is crucial to prevent protein adsorption and to control electroendosmosis [69]. In micro- and nanochannels the surface-to-volume ratio is so high that any molecule sticking to the surface can result in clogging of the channels. It is therefore essential to treat the surfaces in order to minimize non-specific adhesion of biomolecules. Proteins are amphiphilic, positively and negatively charged, making them very likely to adhere to any surface. One very effective way to prevent protein non-specific adsorption is to cover the surface with poly(ethylene glycol) (PEG) [70]. This polymer is neutral, hydrophilic, and very promising in terms of biocompatibility. PEG can be grafted to quartz or glass surfaces using silane-terminated PEG. For elastomer surfaces one can use a poly(ethylene glycol)–poly(propylene oxide)–poly(ethylene glycol) triblock copolymer such as Pluronic F108 (BASF). In aqueous solutions, the hydrophobic poly(propylene oxide) block will self-adsorb onto the elastomer surface, leaving a PEG brush on the surface [71, 72, 73].

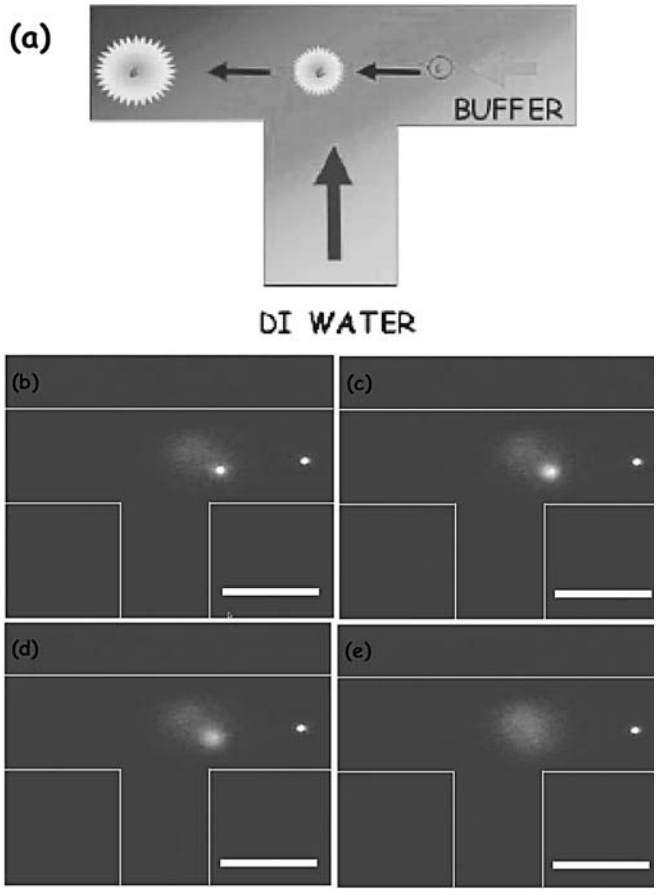

Fig. 6a–e To extract the DNA, the cell is lysed in a diffusion mixer where the cells are introduced from the *right* and water from *below*(**a**). **b–e** An *E. coli* cell is introduced from the *right* and lysed by osmotic shock; the total time from (**b**) to (**e**) is one second. The *scale bars* are 50 μm (from ref. [81] by permission of The Royal Society of Chemistry)

Examples of devices

To study single cells one by one with respect to their contents, a device is envisioned with the following functionalities integrated in sequence on a single chip: (1) cell sorting; (2) cell lysis; (3) extraction of the components of interest such as DNA; (4) purification of the DNA; (5) fractionation of the DNA; (6) analysis of the DNA. In the following we will go through a few examples in connection with each one of these steps, focusing on DNA.

Cell sorting, cell lysis, and DNA extraction

Cells of interest can be sorted on a chip from whole populations based on, for example, their mechanical properties [74, 75, 76], dielectric properties [77, 78], or by specific binding of antibodies attached to various tags [79, 80]. The size scale of the features in such a device is essentially determined by the size range of the cells of interest. Bacteria are typically a few microns in size, whereas eukaryotic cells are tens of microns in size.

Once a cell of interest has been selected and captured, it is lysed to access its contents for further analysis, in our case primarily the DNA. One way of lysing cells is to osmotically shock the cells with pure water. This was demonstrated with osmotically unstable *E. coli* mixed with water in a diffusion mixer [81]. The cells lysed upon contact with the water (Fig. 6), and the DNA was later trapped downstream in a dielectrophoretic trap while the remaining debris was washed away.

Dielectrophoresis

Dielectrophoresis (DEP) [82] is the movement of polarizable or polar particles in non-homogenous electric fields. The applied field is generally an AC field and the resulting force is given by $F_{\mathrm{DEP}} = \alpha\nabla|E|^2$ where α depends on the frequency of the applied electric field (E), the dielectric properties of the particle, and the medium. The force may be attractive or repulsive depending on the properties of the particle and the frequency of the applied electric field. If the particle is more polarizable than the surround-

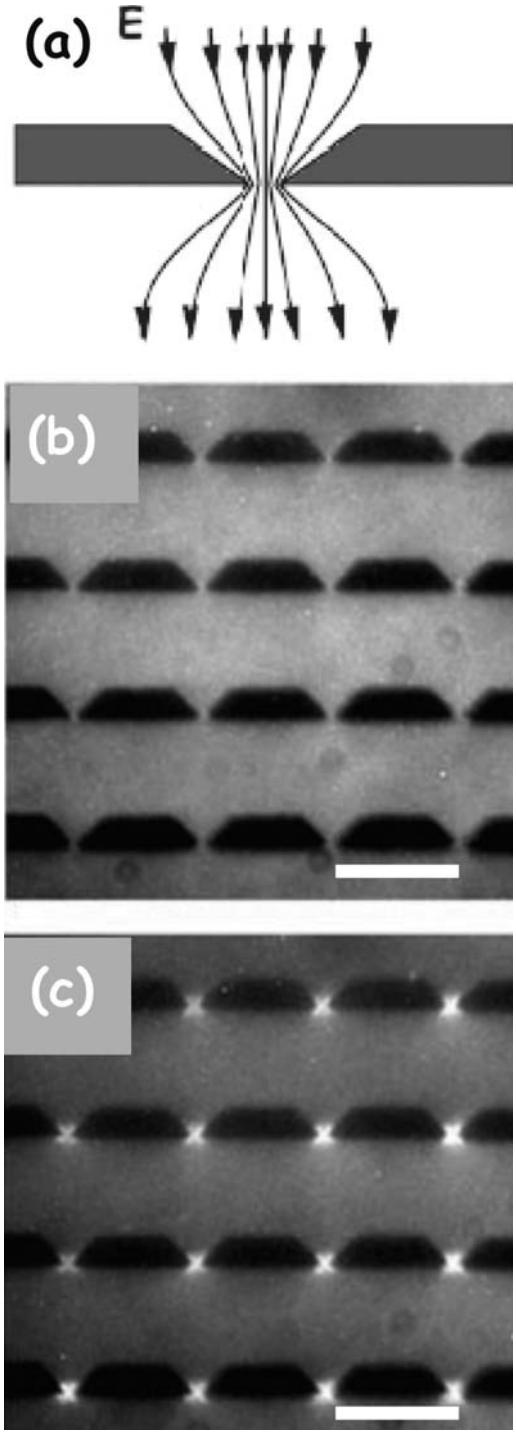

Fig. 7 **a** The required electric field gradient is created by constricting the field in a small gap in a dielectric material (quartz). **b** No voltage is applied over the device and no DNA (386 bp stained with TOTO-1) is detected. **c** An AC voltage is applied and the DNA concentrated in the traps. The *scale bars* are 20 μm (from ref. [88] with permission from The Biophysical Society)

ing medium, the particle will experience an attractive force towards high-field regions. Conversely, if the medium is more polarizable, the particle will experience a repulsive force. Experimentally, the electric field gradients are often realized using metal electrodes [83, 84]. Because of possible electrochemical reactions, the applied voltages are often restricted to low voltages and high frequencies to avoid bubble formation. By using free-floating electrodes [85, 86] electrochemical reactions are no longer a major problem. Still, biomolecules adsorb to the electrodes and may denature. We solved both problems by squeezing the electrical field with dielectric obstacles in a microfluidic channel (Fig. 7a) and applying an AC voltage using electrodes that were external to the chip [87, 88]. Independently, Cummings and coworkers used a similar approach to study dielectrophoresis under a DC electric field [89].

Dielectrophoresis is a very powerful technique used for manipulating and separating [90] molecules [83, 91, 92], virus particles [93, 94, 95, 96], and whole cells [84, 97, 98], and has even been used to separate carbon nanotubes [99]. In the simplest separation device the particles are moved over a surface in a microfluidic channel with integrated electrodes. An AC electric field is applied between the electrodes, and for the appropriate choice of frequency the particles of interest are trapped on the electrodes and can be collected once the remaining particles have been rinsed out. Another idea is to create a microfluidic channel in which the particles are weakly trapped in an array of electrodes creating a potential slope with dips whose depth is dependent on the dielectric properties of the particle. The end result is a device with which particles with different dielectric properties can be separated based on their different mobilities [90].

Another important application of DEP is the fact that it can be used to concentrate particles that would otherwise be difficult to detect [86]. At equilibrium the ratio φ between the concentration of the DNA in the trap and outside the trap is given by the Boltzmann factor $\phi = \exp\left[\alpha\left(E_1^2 - E_0^2\right)/kT\right]$ where α is the effective polarizability of the particle in the solution, E_1 is the electric field in the trap, and E_0 is the electric field outside the trap. In our device [88] we demonstrate this principle by introducing a dilute DNA solution into the channels (Fig. 7b–c). With an applied AC field the DNA can be concentrated and is now clearly visible. This can be useful, for example, to increase the sensitivity of fluorescence-based hybridization assays [100], and to accelerate polymerase chain reaction (PCR) in femtoliter volumes.

DEP can be used to study the behavior of very concentrated solutions locally where the reagents are scarce, provided of course that the reagents are polar or polarizable. By trapping – to a varying degree – DNA in a dielectrophoretic trap, hybridization dynamics can be studied as a function of concentration. A continuous range of concentrations is available by changing the applied voltage over the device rather than preparing a dilution series in test tubes.

For large trapping forces in dielectrophoresis, high electric fields are desirable. This can be achieved by creating very sharp electrodes or it can be realized using small constrictions. The practical limit is determined by the relevant breakdown fields of the buffers used and of the dielectric materials used. To avoid clogging, the size of the

constrictions cannot be exceeded by the size of the particles, which for large DNA molecules and cells amounts to roughly a micron.

Fractionation of DNA

Fractionation of DNA is a fundamental experimental technique in molecular biology for measurement of size (e.g., sequencing) and mobility distributions (e.g., gel shift assays for protein–DNA interactions) of DNA samples, as well as preparation of fractions of DNA samples (e.g., BAC or PAC libraries) for further experiments. There are however limitations to conventional techniques. Standard gel electrophoresis is capable of separating DNA molecules up to around 40 kbases, above which the mobility becomes independent of the size due to the stretching of the DNA. Separating larger, chromosome-size DNA takes anything from days to weeks using pulsed-field gel electrophoresis [19, 101]. Capillary electrophoresis has been shown to separate megabase-size DNA in 10 min [102]. However, only one sample per capillary can be run, harvesting the sample is difficult, and aggregation of the DNA due to electrohydrodynamic instabilities makes it unreliable [103]. In addition, to integrate gel-filled capillaries in a microfabricated system is not trivial. These problems are solved by defining structures in microfluidic channels that either consist of obstacle courses, by analogy with gels, or that allow direct measurement of the lengths of the DNA. In this way the speed of separation is increased significantly and the devices can easily be integrated into a complete on-chip analysis system.

The most straightforward approach to measuring the size of DNA molecules in a microfluidic channel is simply by measuring the resulting fluorescent light emitted from individual, stained DNA [104, 105]. With uniformly stained DNA, the amount of emitted light is proportional to the size of the DNA molecule. In this way Foquet et al. were able to determine the size distribution of a DNA sample of less than 100 fg in a few minutes [104]. This can be compared to the several nanograms and the several days that are required in standard pulsed-field gels [19, 101, 106, 107]. Another device for direct fluorescence measurements and sorting of DNA molecules was constructed from PDMS by Quake's group [105].

There is a wide range of obstacle-course designs defined in microfluidic environments that have been used for DNA separation. In most of them, the DNA interacts sterically with obstacles defined in a microfluidic channel making it necessary to fabricate the devices with feature sizes on the order of or smaller than the root mean square of the length of the end-to-end vector of the DNA, given by $R_{\mathrm{RMS}}^2 = L\,b$ (ignoring excluded volume effects), where L is the contour length and b, the Kuhn length at standard buffer conditions, is approximately 100 nm. For lambda phage DNA (48.5 kbp) we have $R_{\mathrm{RMS}} \approx 1.3\,\mu\mathrm{m}$ (using 0.34 nm per base pair for B-DNA).

One example of an obstacle-course design is based on entropic barriers where a microfluidic channel is defined with a sequence of deep and shallow channels. Here the mobility of DNA is larger for large molecules than for small ones, and DNA molecules up to 200 kbp have been separated in 30 min [108, 109, 110]. Another example is based on entropic recoil [111], where DNA is moved into small channels using a train of voltage pulses. While the voltage is switched on, the DNA is moved into the channel. While the voltage is switched off, any molecules entirely within the channels will remain in the channels, whereas those that have any region outside the channel will relax back into the bulk liquid, gaining entropy. Since small molecules have a larger probability of being entirely within the channels, they will not relax back and their effective mobility in the device will be larger.

By mimicking a standard gel with posts arranged in a hexagonal pattern in a microfluidic channel, we were able to separate chromosome-size DNA molecules in a few seconds. The principle is very simple. An electrical field driving the DNA is applied alternately in two different directions separated by 120° for optimum performance (Fig. 8) [20, 21, 112]. As the electric field is shifted the DNA must backtrack its entire length in the new direction. After the DNA has completely backtracked, the remaining movement of the DNA during the half-period constitutes the effective displacement of the DNA and depends on the length of the DNA. The applied voltage and frequency of the oscillations is chosen so that the desired range of DNA lengths are separated. This approach has been able to a achieve separation of 100-kbp DNA molecules in 10 s [20], which is several orders of magnitude faster than conventional slab gel approaches [19] and an order of magnitude faster than pulsed-field capillary electrophoresis [102].

Separation performance is limited by the achievable resolution, which in turn depends on the width of the initial band of DNA and how regularly the DNA moves in the array. A narrow band can be defined by dielectrophoretic trapping of the DNA onto a free-floating metallic wire [85]. This limits the amount of DNA that can be assayed at each time and there is also a risk that biomolecules bind to the metal and denature. An entropic barrier is another alternative [20]. In this case, the DNA is collected at the barrier with a small voltage after having been pulled through the barrier with a higher voltage. After collection into a thin band, the DNA is introduced into the device by reversing the voltage. A more elegant approach is to introduce the DNA as a hydrodynamically or electrically focused "jet" into the array [113]. It is generally important to keep in mind that microfluidic devices work in the low-Reynolds-number regime and that inertia is negligible. This means that sample injection cannot rely on inertia to define a narrow band. Instead, a uniform fluid flow or electric current must be defined using a large number of parallel sources, one of which provides the DNA. If the flows or the currents are tuned carefully, a narrow band and a uniform field is the result [113]. In this way the movement of DNA in the array can be precisely controlled and the resolution is enhanced.

In the abovementioned devices the DNA is moved in a steady stream, and the size is determined by measuring its

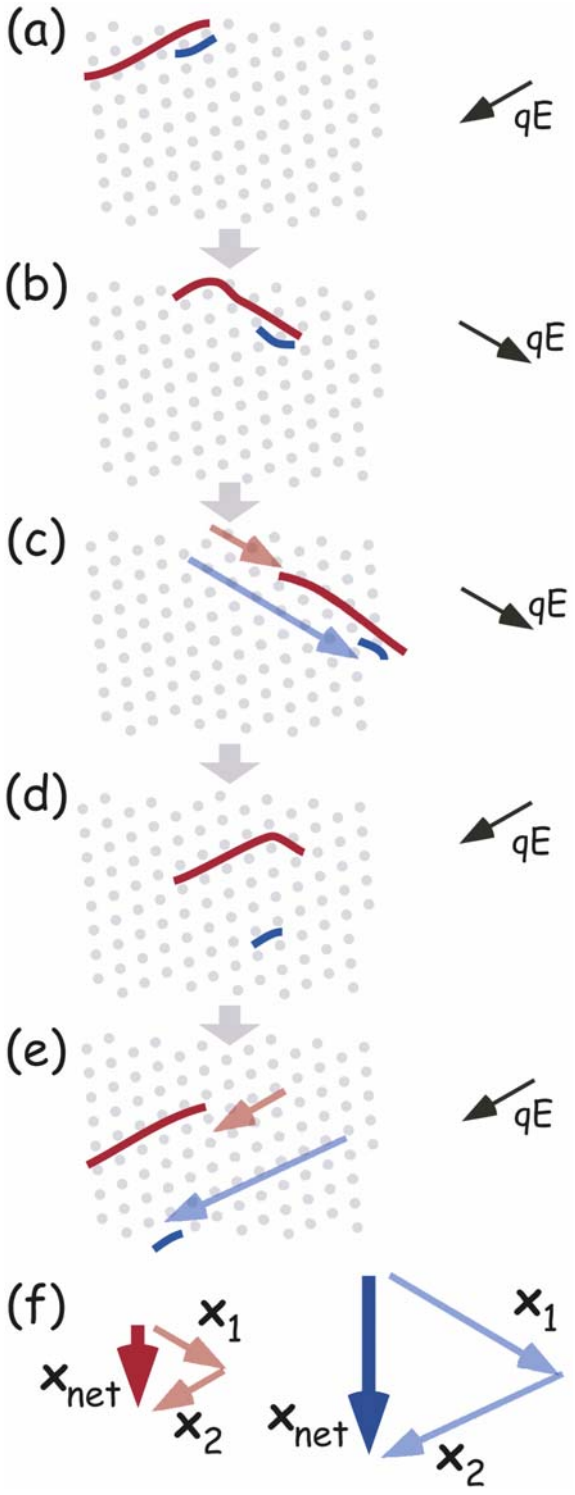

Fig. 8 a–e One small (*blue*) and one large (*red*) DNA molecule is pulled in two alternating directions separated by 120°. The *arrow* labeled *qE* denotes the applied driving force (electric field). In **c** and **e** the *arrows* in the array show the net motion of the DNA for each half period. The vector sum of the displacements during each half period ($\mathbf{x}_1$ and $\mathbf{x}_2$) gives the net displacement ($\mathbf{x}_{net}$) for one full cycle (**f**) for the large (*left*) and the small (*right*) molecule. During one period the small molecule has moved a greater distance than the large molecule and the effective mobility of DNA in the array is thus a decreasing function of length

fluorescence or its mobility. To be useful for preparative assays where larger amounts are desired, separation need to occur in *space*. We were able to achieve this with a slight modification of the approach described in ref. [20] and above in Fig. 8. By using electric fields with one of the two pulses longer or stronger than the other instead of symmetric electric field pulses, the result is separation of DNA not only in time, but also spatially (Fig. 9) [21]. In this way we created a "DNA prism" that can run continu-

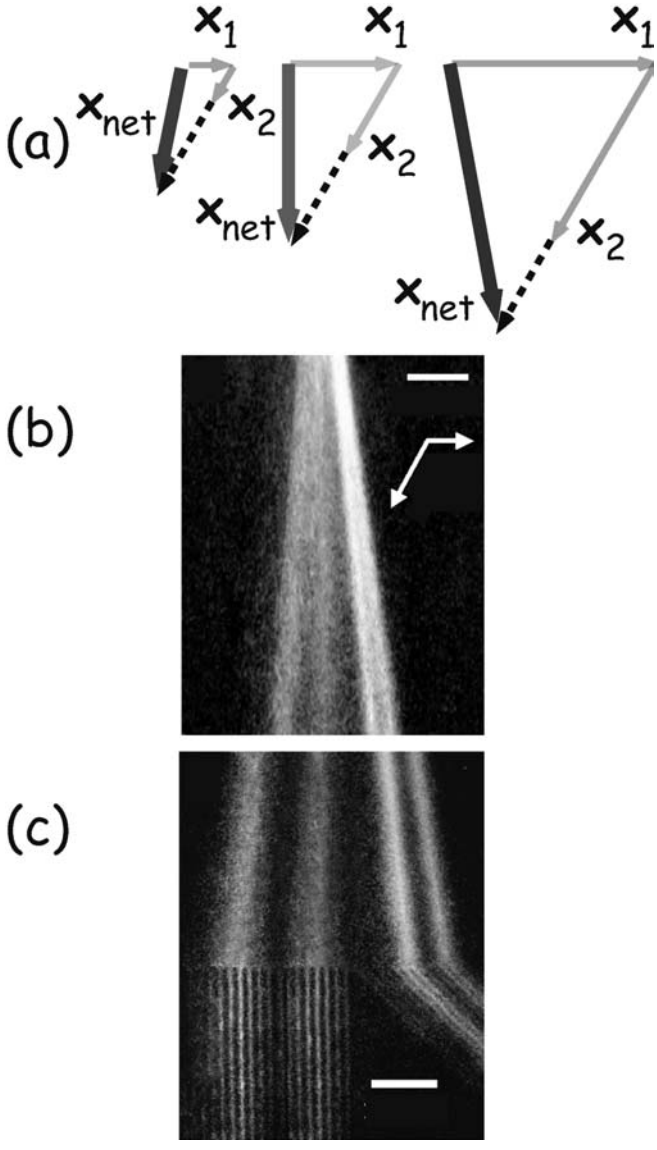

Fig. 9 **a** To achieve a separation in space, a bias (*dashed arrow*) is added to the applied driving force (electric field) so that the DNA moves a longer distance in one of the half periods. The result is DNA that moves in an angle that is a function of the size of the DNA molecules. The result for the largest DNA is depicted to the *left* and for the smallest DNA to the *right*. In **b** and **c** actual DNA is separated into different reservoirs for possible further analysis. The size of the DNA in the four bands is (from *left* to *right*): 209 kbp, 158 kbp, 114 kbp, and 61 kbp. The *scale bar* is 200 µm (**b** and **c** are reproduced from ref. [21] with permission from The Nature Publishing Group)

ously, and nanograms of DNA can be separated per hour. This may seem to be a small amount by present-day standards, although the quantity in any case is sufficient for sequencing libraries. Nevertheless, the goal is to integrate the fractionation device in a chip-based system where only small amounts of reagents are necessary.

Another continuous separation scheme is based on a Brownian ratchet [114, 115]. The basic idea is to use a regular array of asymmetric obstacles to rectify the Brownian motion laterally and thereby deflect diffusing particles depending on their size. The idea has been realized for separation of DNA [116] and phospholipids [117]. By appropriate scaling of the device, it can be used for separation of other particles and molecules such as whole cells, organelles, proteins, and viruses. The basic design requirements are discussed elsewhere [118, 119]. Essentially, the obstacle spacing a should be such that the Péclet number, $Pe = \frac{va}{D}$, is of the of order unity. Here v is the velocity and D is the diffusion coefficient of the particles. It was later realized [120] that for devices with obstacles that are impermeable to the electric field, there can be no separation unless the particles have a finite size of the order of the obstacle spacing. For lambda phage DNA (48.5 kbp), for example, the required post spacing for typical velocities is close to a micron.

Linear analysis of DNA

DNA is a linear molecule and a significant amount of information is organized linearly along the DNA (e.g., length, sequence, and epigenetic and genetic modifications). The length can quickly be measured simply by stretching and immobilizing the DNA on a surface [121]. This is useful for restriction mapping [122]. For high-throughput devices it is more desirable to allow the DNA to move through the channels and only intermittently stop the DNA for analysis. In this case other approaches must be taken to stretch the DNA, which we now discuss.

Our ultimate goal is to not only be able to measure the lengths of individual DNA molecules, but also to detect fluorescent labels attached to the DNA at specific genetic sequences using hybridization probes, at methylation sites, or at proteins such as transcription factors bound to the DNA. We understand that we cannot obtain a full picture of the transcriptional regulation using linear analysis of DNA, since many times loops of the DNA and other more complicated structures are involved. On the other hand, devices to approach the problem can be envisioned, since the size range of the control complexes, on the 20-nm scale, is accessible using nanotechnology.

Direct readout of fluorescent labels along the DNA can be achieved for DNA stretched on a surface; however, other approaches are necessary for high-precision localization of labels that are situated very closely. There are two fundamental requirements: (1) the optical resolution needs to be on the scale of the features of interest, namely, ranging from single bases (0.34 nm) to binding sites for control factors (20 bp≈10 nm), to individual genes (1 kbp≈0.3 μm) and upwards; (2) the DNA needs to be stretched uniformly over the length of interest so that a measured distance in space can be interpreted in terms of number of base pairs, which is the relevant biological length scale.

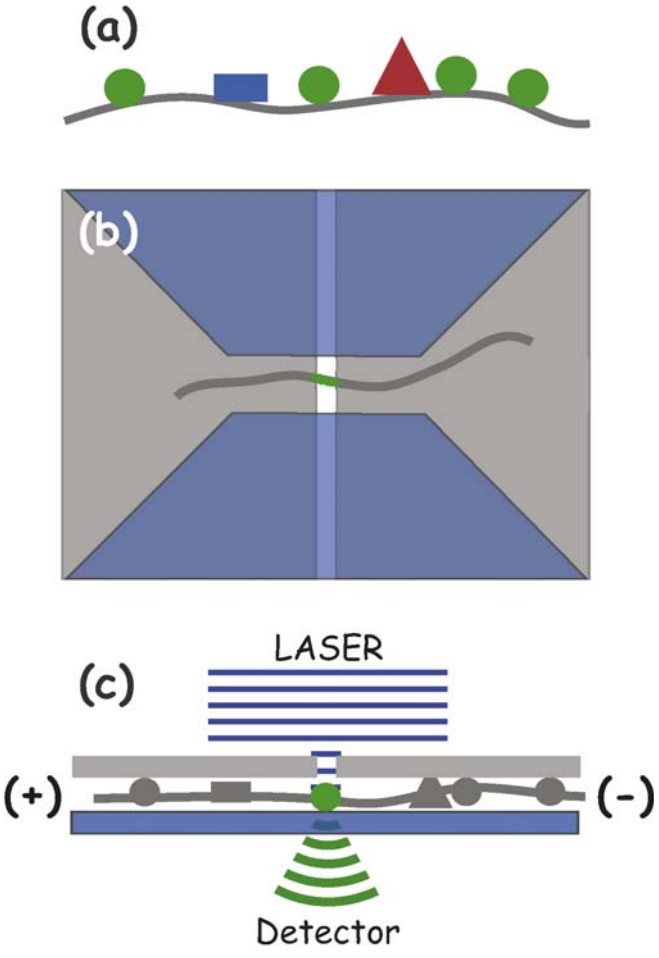

Fig. 10 **a** Linear analysis of DNA. The idea is to detect the occurrence and the locations of fluorescent tags attached to the DNA. **b** A nearfield chip is envisioned with microfluidic channels defined on top of an aluminum film with integrated slit-shaped apertures. A laser focused on the opposite side results in an evanescent field in the channel providing the basis for high-resolution imaging. **c** Side-view of the device with the DNA in the microfluidic channel

To achieve high optical resolution, nearfield optics is the natural choice. It overcomes the diffraction limit imposed on standard microscopy, and can be realized by integrating local point sources of light in the fluidic channels. To this end we made a nearfield-based device on a chip [123]. It consists of a microfluidic channel with posts for stretching the DNA and integrated slits defined in a metallic film and oriented perpendicularly to the microfluidic channel (Figs. 10 and 11). Two problems became evident using this device: the optical resolution, although 200 nm, could be vastly improved, and the DNA was poorly stretched using the posts. The key is to use nanofluidics to address both problems.

The micron-scale channel used in our nearfield device [123] did not sufficiently confine the DNA in close prox-

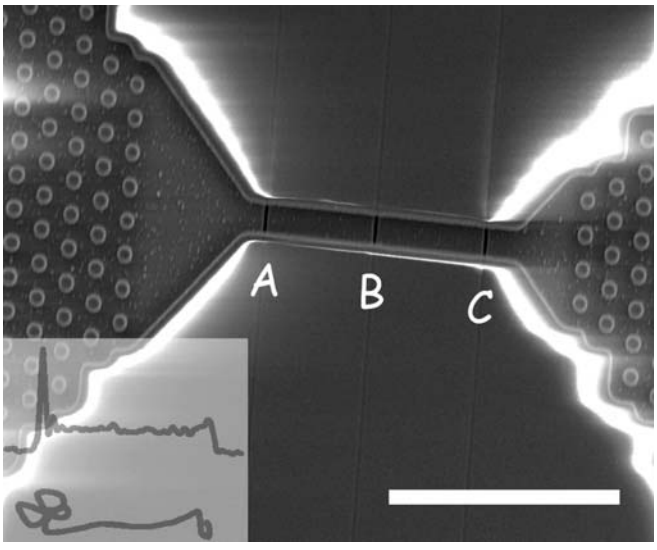

Fig. 11 The nearfield chip in ref. [123] fabricated with microfluidic channels on top of an aluminum film with integrated slit-shaped apertures denoted by *A*, *B*, and *C*. A post array was fabricated on either end of channel. The *scale bar* is 20 µm. The *inset* is the time trace (*top*) of the fluorescence as a result of one DNA molecule passing through the device together with a sketch (*bottom*) of the corresponding DNA conformation. Note the large initial peak, which corresponds to the disordered head of the molecule

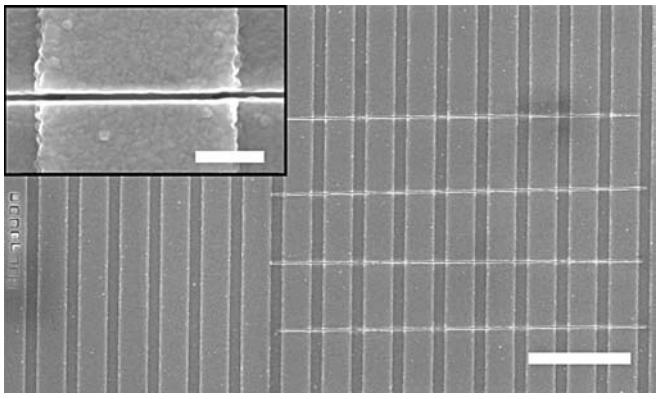

Fig. 12 An aluminum film deposited on fluidic channels. 40-nm-wide apertures were defined in the aluminum film using focused ion beam (FIB) milling. The *insert* shows a magnified section of a nanoslit defined in the aluminum film on top of a fluidic channel. The *scale bar* is 5 µm (500 nm in the *inset*) (JO Tegenfeldt and P Silberzan, unpublished work. At Princeton University YM Wang continues the work)

imity to the aperture. This resulted in poor resolution. For high-resolution nearfield excitation it is crucial that the sample be as close as possible to the light source [124, 125, 126]. Typically, to achieve a resolution of less than 100 nm, the sample must be positioned within less than 100 nm of the light source. Nanoscale channels can be used to confine the sample to the immediate vicinity of the light source. To make alignment of a stretched DNA to the light source easier, a slit is defined rather than a hole. An example of an aperture made using FIB in an aluminum film on buried nanochannels is shown in Fig. 12. While good resolution can be achieved, limited by the skin depth of the metal film, the transmission of light through sub-wavelength apertures is in general very low. To improve the transmission, an effect explored by Thio, Ebbesen, and coworkers can be utilized [127]. In their work, the authors defined small indentations in a periodic pattern around the aperture. Such perturbations couple to the surface plasmons in the metal film and improve the transmission significantly. Instead of using apertures, small LEDs, lasers, or passive fluorescent particles such as quantum dots [128, 129] can be utilized. A further alternative is to position metallic particles for local field enhancement [130, 131, 132] in the channels. Many of these excitation sources can be made point-like, down to a few nanometers, opening up the possibility for unprecedented optical resolution on a chip, provided the sample can be positioned from the source a distance not exceeding the desired resolution.

The stretching in our device [123], using intermittent attachment at a post, will result in a tension in the DNA that is greatest at the tethered end and essentially zero at the free end, resulting in a very non-uniform stretching [133]. Uniform stretching can only be realized if each segment of the DNA experiences the same driving force, for example, in the confinement of a small channel. An important requirement for uniform stretching is that no loops form. To avoid loops due to thermal fluctuations, the diameter (D) of the channels need to be close to or less than the persistence length of the DNA [134, 135], $L_p \approx 50$ nm, so that the energy $U = \pi k_B T \frac{L_p}{R}$ required to form a loop of radius $R \approx D/2$ is greater than the thermal energy $k_B T$, where k_B is the Boltzmann constant, and T is the absolute temperature. The results of our first experiments with DNA in 100-nm-diameter channels show DNA in a uniformly stretched configuration (Fig. 13).

To demonstrate the sizing capabilities of direct visualization of DNA in nanochannels, we studied TOTO-1 (Molecular Probes, OR) stained lambda phage DNA in 100-nm-diameter channels made by nanoimprinting lithography [30]. The stretched DNA molecules were imaged using standard epifluorescence microscopy, and the lengths of the molecules were measured by direct inspection and analyzed using a standard image analysis software package [136]. The width of the resulting size distribution is comparable to that achievable using standard slab electrophoresis (Fig. 14), although in our case the data acquisition took just a few minutes and required considerably less DNA. Gel electrophoresis typically requires five or more nanograms of DNA per molecular weight species. We used only approximately 1,000 lambda phage molecules, corresponding to 50 fg, which is seven orders of magnitude less. By averaging many frames, the length can in principle be determined to a precision of a few nanometers, limited by the number of photons that can be extracted from the dyes used to label the DNA [137, 138].

The prospects of extracting DNA from a single cell and probing the DNA linearly from one end to the other

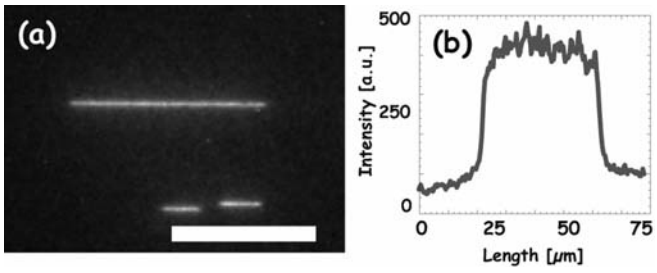

Fig. 13 A long DNA (a pentamer of lambda phage DNA) stretched uniformly in a 100 nm×100 nm channel. The DNA was stained with TOTO1 fluorescent dye (Molecular Probes, Eugene, OR) imaged in an epifluorescence microscope using a IPentaMax ICCD (Roper Scientific, Trenton, NJ) and electrophoretically moved into the array. The *scale bar* is 30 μm (JO Tegenfeldt and H Cao, unpublished work. At Princeton University R Riehn, WW Reisner, and YM Wang continue the work)

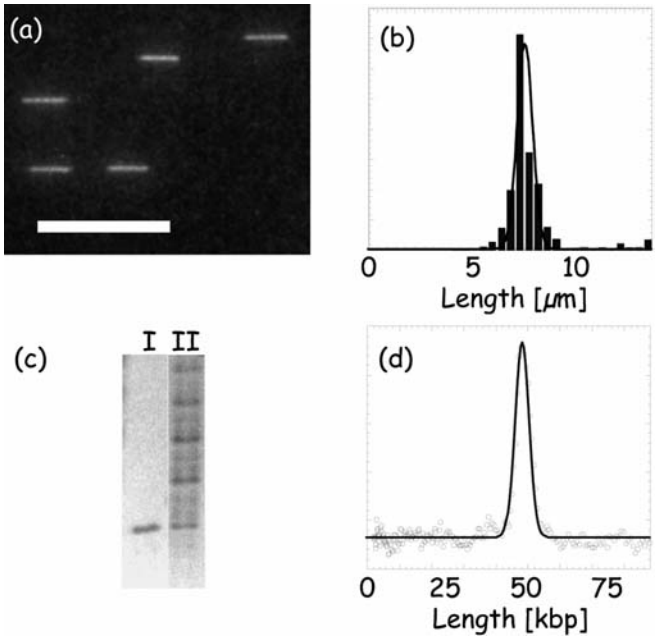

Fig. 14 **a** Lambda phage DNA spontaneously stretches out in a nanochannel array where the channels have a cross section of 100 nm. The DNA was stained with TOTO1 fluorescent dye (Molecular Probes, Eugene, OR) imaged in an epifluorescence microscope using a IPentaMax ICCD (Roper Scientific, Trenton, NJ) and electrophoretically moved into the array. The *scale bar* is 25 μm. **b** By measuring the lengths of the individual DNA molecules that pass through the nanochannel array, an estimate of the size distribution can be obtained. A histogram is formed with the amount of DNA as a function of length. A Gaussian is fitted to the distribution with an average of x=7.5 μm and a standard deviation of σ=0.4 μm. **c** The lambda phage DNA is analyzed in a standard gel (*lane I*) which is calibrated using a lambda ladder (*lane II*). **d** A Gaussian is fitted to the density profile of the readout of the gel with an average of x=48.5 kbp and a standard deviation of σ=2 kbp (JO Tegenfeldt, unpublished work. At Princeton University R Riehn, WW Reisner, and YM Wang continue the work)

depend on what organism is studied. Bacteria (prokaryotic cells) have a relatively simple structure with loosely packaged DNA with a low content of associated protein. For these organisms it should be fairly straightforward to extract and analyze the DNA. In the more complex cells from higher organisms (eukaryotic cells) the DNA is packaged more densely with a large amount of protein. For these cells any necessary separation of the DNA from histones and other proteins presents a challenge. On the other hand, the compartmentalization of the eukaryotic cell offers an advantage. After cell lysis, the organelles, where the DNA is present, such as the nucleus and mitochondria, are separated. Then the DNA from each organelle can be treated separately, which simplifies the subsequent DNA extraction, purification, and identification.

Summary and outlook

We have reviewed a selection of device components, some of which have shown a remarkable improvement over traditional techniques with respect to speed and reagent consumption. To make an even larger impact and really profit from the advantages of miniaturization, we need to go further and integrate these components into a complete system. In that way we could fully analyze single cells with respect to their contents. Just as the field of single-molecule studies has revealed a wealth of new information we expect that single-cell biochemistry [139] will do the same.

To make the devices fully versatile and to take advantage of the capability of parallel processes, detection and signal-processing systems must be integrated on-chip. To probe biology on the scale of its basic building blocks, we need to develop single-molecule detection capability with single-nanometer spatial resolution *integrated* in nanofluidic chips. There is an enormous potential in the microelectronics and telecommunications industry to create very complex devices with integrated signal processing (e.g., optical excitation, manipulation and detection, electrical and magnetic manipulation and detection). The challenge is to adapt this technology to biological applications, where buffer solutions contain ions that can poison the components and render them useless.

In shrinking bioanalytical devices from the micron regime to the nanometer regime, we face a few fundamental challenges that need to be addressed. As the dimensions are decreased, the surface-to-volume ratio increases, and surface effects become increasingly important. Unless the surfaces are properly passivated, contaminants will adsorb to the walls of the fluidic channels affecting the performance of the device. Another challenge is fluid and sample transport. Due to the stick boundary conditions for pressure-driven flow, the required pressures become impractical for very small channels. Clever design of the fluidic network combining small and large channels is necessary. Electrokinetic transport and other alternatives to pressure-driven flow need to be utilized.

Acknowledgments The authors are indebted to Zhaoning Yu for making high-quality nanostructured surfaces using nanoimprinting lithography. The authors are especially indebted to the following colleagues for fruitful discussions. Olgica Bakajin, Lawrence Livermore National Laboratories, CA; Shirley S. Chan, Princeton, NJ; Prof Chia-Fu Chou, Arizona State University, Tempe, AZ; Prof H.

C. Craighead at Cornell, Ithaca, NY; Nicholas C. Darnton at the Rowland Institute at Harvard, Cambridge, MA; Thomas A.J. Duke at Cavendish Laboratory, Cambridge, UK; J.J. Kraeft, Princeton University, NJ; Robert Riehn, Princeton University, NJ; Walter W. Reisner, Princeton University, NJ; Pascal Silberzan at the Institut Curie, Paris, France; and Yan Mei Wang, Princeton University, NJ.

The work was funded by grants from the Defense Advanced Research Projects Agency (MDA972–00–1-0031), the National Institutes of Health (HG01506), the state of New Jersey (NJCST 99–100–082–2042–007), and the Nanobiotechnology Center (NSF BSCECS9876771).

References

1. Campbell NA (1996) Biology, 4th ed. Benjamin/Cummings, Menlo Park
2. Stryer L (1995) Biochemistry, 4th ed. Freeman, New York
3. Ptashne M (1992) A genetic switch: phage lambda and higher organisms, 2nd ed. Blackwell, Cambridge, MA
4. Ptashne M, Gann A (2002) Genes and signals. Cold Spring Harbor Laboratory Press, Cold Spring Harbor, NY
5. Hoch HC, Jelinski LW, Craighead HC (eds) (1996) Nanofabrication and biosystems: integrating materials science, engineering, and biology. Cambridge University Press, Cambridge, UK
6. Craighead HG (2000) Nanoelectromechanical systems. Science 290:1532–1535
7. Manz A, Graber N, Widmer HM (1990) Miniaturized total chemical-analysis systems – a novel concept for chemical sensing. Sens Actuators B 1:244–248
8. Lockhart DJ, Winzeler EA (2000) Genomics, gene expression and DNA arrays. Nature 405:827–836
9. Larson CJ, Verdine GL (1996) The chemistry of protein-DNA interactions. In: Hecht SM (ed) Bioorganic chemistry: nucleic acids. Oxford University Press, New York, NY, pp 324–346
10. Wolffe A (1998) Chromatin, structure and function, 3rd ed. Academic Press, London
11. Li E, Beard C, Jaenisch R (1993) The role of DNA methylation in genomic imprinting. Nature 366:362–365
12. Dennis C (2003) Altered states. Nature 421:686–688
13. Tilghman SM (1991–2) Parental imprinting in the mouse. The Harvey Lectures 87:69–84
14. Chicurel M (2001) Faster, better, cheaper genotyping. Nature 412:580–582
15. Wall JD, Pritchard JK (2003) Haplotype blocks and linkage disequilibrium in the human genome. Nature Rev Genet 4(8): 587–597
16. Goldstein DB (2001) Islands of linkage disequilibrium. Nature Genet 29:109–111
17. Kwok PY (2001) Methods for genotyping single nucleotide polymorphisms. Annu Rev Genomics Human Genet 2:235–258
18. Schwartz DC, Li XJ, Hernandez LI et al (1993) Ordered restriction maps of saccharomyces-cerevisiae chromosomes constructed by optical mapping. Science 262:110–114
19. Cox EC, Vocke CD, Walter S et al (1990) Electrophoretic karyotype for Dictyostelium discoideum. Proc Natl Acad Sci USA 87:8247–8251
20. Bakajin O, Duke TAJ, Tegenfeldt J et al (2001) Separation of 100-kilobase DNA molecules in 10 seconds. Anal Chem 73(24):6053–6056
21. Huang LR, Tegenfeldt JO, Kraeft J et al (2002) A DNA prism for high-speed continuous fractionation of large DNA molecules. Nature Biotechnol 20(10):1048–1051
22. Madou MJ (2002) Fundamentals of microfabrication: the science of miniaturization, 2nd ed. CRC Press, Boca Raton, FL
23. Campbell SA (1996) The science and engineering of microelectronic fabrication. Oxford University Press, New York
24. Moore GE (1965) Cramming more components onto integrated circuits. Electronics 38(8):114–117
25. Intel Corporation (2003) http://www.intel.com/research/silicon/lithography.htm. Cited 4 Nov 2003
26. Chapman HN, Ray-Chaudhuri AK, Tichenor DA et al (2001) First lithographic results from the extreme ultraviolet engineering test stand. J Vac Sci Technol B 19(6):2389–9235
27. Naulleau P, Goldberg KA, Anderson EH et al (2002) Sub-70 nm extreme ultraviolet lithography at the advanced light source static microfield exposure station using the engineering test stand set-2 optic. J Vac Sci Technol B 20(6):2829–2833
28. Junno T, Deppert K, Montelius L et al (1995) Controlled manipulation of nanoparticles with an atomic force microscope. Appl Phys Lett 66(26):3627
29. Eigler DM, Schweizer EK (1990) Positioning single atoms with a scanning tunneling microscope. Nature 344:524–526
30. Chou SY, Krauss PR, Renstrom PJ (1996) Imprint lithography with 25-nanometer resolution. Science 272:85–87
31. Chou SY, Krauss PR, Zhang W et al (1997) Sub-10 nm imprint lithography and applications. J Vac Sci Technol B 15(6): 2897–2904
32. Heidari B, Maximov I, Montelius L (2000) Nanoimprint lithography at the 6 in wafer scale. J Vac Sci Technol B 18(6):3557–3560
33. Smith HI (2001) Low cost nanolithography with nanoaccuracy. Phys E Low-Dimension Syst Nanostructures 11(2–3): 104–109
34. Solak HH, David C, Gobrecht J et al (2002) Multiple-beam interference lithography with electron beam written gratings. J Vac Sci Technol B 20(6):2844–2848
35. Solak HH, David C, Gobrecht J et al (2003) Sub-50 nm period patterns with EUV interference lithography. Microelectron Eng 67–68:56–62
36. Mansky P, Harrison CK, Chaikin PM et al (1996) Nanolithographic templates from diblock copolymer thin films. Appl Phys Lett 68(18):2586–2588
37. Harrison CK, Adamson DH, Park M et al (1997) Lithography with a mask of block copolymer microstructures. Abstr Papers Am Chem Soc 214:116-PMSE
38. Park M, Harrison C, Chaikin PM et al (1997) Block copolymer lithography: periodic arrays of similar to 10(11) holes in 1 square centimeter. Science 276:1401–1404
39. Adamson DH, Harrison C, Park M et al (1998) Towards control and optimization of diblock copolymer microphases. Abstr Papers Am Chem Soc 216:062-MACR
40. Harrison C, Park M, Chaikin PM et al (1998) Lithography with a mask of block copolymer microstructures. J Vac Sci Technol B 16(2):544–552
41. Register RA, Park M, Adamson DH et al (1999) Nanolithography with a block copolymer mask: fabrication of a dense metal dot array. Abstr Papers Am Chem Soc 218:7-PMSE
42. van Blaaderen A, Ruel R, Wiltzius P (1997) Template-directed colloidal crystallization. Nature 385:321–324
43. Vlasov YA, Bo XZ, Sturm JC et al (2001) On-chip natural assembly of silicon photonic bandgap crystals. Nature 414:289–293
44. Tong Q-Y, Gösele U (1998) Semiconductor wafer bonding: science and technology. Wiley
45. Ju S-P, Weng C-I, Chang J-G et al (2002) Molecular dynamics simulation of sputter trench-filling morphology in damascene process. J Vac Sci Technol B 20(3):946–955
46. Cao H, Yu Z, Wang J et al (2002) Fabrication of enclosed nanofluidic channels. Appl Phys Lett 81(1):174–176
47. Turner SW, Perez AM, Lopez A et al (1998) Monolithic nanofluid sieving structures for DNA manipulation. J Vac Sci Technol B 16(6):3835–3840
48. Reed HA, White CE, Rao V et al (2001) Fabrication of microchannels using polycarbonates as sacrificial materials. J Micromech Microeng 11(6):733–737

49. Harnett CK, Coates GW, Craighead HG (2001) Heat-depolymerizable polycarbonates as electron beam patternable sacrificial layers for nanofluidics. J Vac Sci Technol B 19(6): 2842–2845
50. Bhusari D, Reed HA, Wedlake M et al (2001) Fabrication of air-channel structures for microfluidic, microelectromechanical, and microelectronic applications. J Microelectromech Syst 10(3):400–408
51. Li W, Tegenfeldt JO, Chen L et al (2003) Sacrificial polymers for nanofluidic channels in biological applications. Nanotechnology 14(6):578–583
52. Quake SR, Scherer A (2000) From micro- to nanofabrication with soft materials. Science 290:1536–1540
53. Love JC, Anderson JR, Whitesides GM (2001) Fabrication of three-dimensional microfluidic systems by soft lithography. MRS Bull 26(7):523–528
54. Anderson JR, Chiu DT, Jackman RJ et al (2000) Fabrication of topologically complex three-dimensional microfluidic systems in PDMS by rapid prototyping. Anal Chem 72(14): 3158–3164
55. McDonald JC, Duffy DC, Anderson JR et al (2000) Fabrication of microfluidic systems in poly(dimethylsiloxane). Electrophoresis 21(1):27–40
56. Unger MA, Chou HP, Thorsen T et al (2000) Monolithic microfabricated valves and pumps by multilayer soft lithography. Science 288:113–116
57. Thorsen T, Maerkl SJ, Quake SR (2002) Microfluidic large-scale integration. Science 298:580–584
58. Delamarche E, Bernard A, Schmid H et al (1997) Patterned delivery of immunoglobulins to surfaces using microfluidic networks. Science 276:779–781
59. Kenis PJA, Ismagilov RF, Whitesides GM (1999) Microfabrication inside capillaries using multiphase laminar flow patterning. Science 285:83–85
60. Brody JP, Yager P, Goldstein RE et al (1996) Biotechnology at low Reynolds numbers. Biophys J 71(6):3430–3441
61. Beebe DJ, Mensing GA, Walker GM (2002) Physics and applications of microfluidics in biology. Annu Rev Biomed Eng 4:261–286
62. Duffy DC, Gillis HL, Lin J et al (1999) Microfabricated centrifugal microfluidic systems: characterization and multiple enzymatic assays. Anal Chem 71(20):4669–4678
63. Taylor G (1953) Dispersaion of soluble matter in solvent flowing slowly through a tube. Proc Royal Soc London Ser A Math Phys Sci 219:186–203
64. Landau LD, Lifshitz EM (1987) Fluid mechanics, 2nd ed. Pergamon, Oxford
65. Hjertén S (1967) Free zone electrophoresis. Chromatogr Rev 9:122–219
66. Liao JL, Abramson J, Hjerten S (1995) A highly stable methyl cellulose coating for capillary electrophoresis. J Capillary Electrophor 2(4):191–196
67. Hjerten S (1985) High-performance electrophoresis – elimination of electroendosmosis and solute adsorption. J Chromatogr 347(2):191–198
68. Gaudioso J, Craighead HG (2002) Characterizing electroosmotic flow in microfluidic devices. J Chromatogr A 971(1–2): 249–253
69. Rodriguez I, Li SFY (1999) Surface deactivation in protein and peptide analysis by capillary electrophoresis. Anal Chim Acta 383(1–2):1–26
70. Milton HJ (ed) (1992) Poly(ethylene glycol) chemistry: biotechnical and biomedical applications. Plenum, New York
71. Caldwell KD (1997) In: Harris JM, Zalipsky S (eds) Surface modifications with adsorbed PEO-based block copolymers: physical characteristics and biological use, in chemistry and biological applications of polyethylene glycol. Am Chem Soc, Washington, 680:400–419
72. Li JT, Carlsson J, Huang SC et al (1996) Adsorption of poly(ethylene oxide)-containing block copolymers – a route to protein resistance. Hydrophilic Polym 248:61–78
73. Webb K, Caldwell KD, Tresco PA (2001) A novel surfactant-based immobilization method for varying substrate-bound fibronectin. J Biomed Mater Res 54(4):509–5018
74. Carlson RH, Gabel CV, Chan SS et al (1997) Self-sorting of white blood cells in a lattice. Phys Rev Lett 79(11):2149–2152
75. Gifford SC, Frank MG, Derganc J et al (2003) Parallel microchannel-based measurements of individual erythrocyte areas and volumes. Biophys J 84(1):623–6233
76. Brody JP, Han YQ, Austin RH et al (1995) Deformation and flow of red-blood-cells in a synthetic lattice – evidence for an active cytoskeleton. Biophys J 68(6):2224–2232
77. Gascoyne PRC, Noshari J, Becker FF et al (1994) Use of dielectrophoretic collection spectra for characterizing differences between normal and cancerous cells. IEEE Trans Ind Appl 30(4):829–834
78. Becker FF, Wang X-B, Huang Y et al (1995) Separation of human breast cancer cells from blood by differential dielectric affinity. Proc Natl Acad Sci USA 92(3):860–864
79. Berger M, Castelino J, Huang R et al (2001) Design of a microfabricated magnetic cell separator. Electrophoresis 22(18): 3883–3892
80. Fu AY, Chou HP, Spence C et al (2002) An integrated microfabricated cell sorter. Anal Chem 74(11):2451–2457
81. Prinz C, Tegenfeldt JO, Austin RH et al (2002) Bacterial chromosome extraction and isolation. Lab Chip 2:207–212
82. Pohl HA (1978) Dielectrophoresis. Cambridge University Press, Cambridge
83. Washizu M, Suzuki S, Kurosawa O et al (1994) Molecular dielectrophoresis of biopolymers. IEEE Trans Ind Appl 30(4): 835–843
84. Morgan H, Hughes MP, Green NG (1999) Separation of submicron bioparticles by dielectrophoresis. Biophys J 77(1): 516–525
85. Asbury CL, van den Engh G (1998) Trapping of DNA in nonuniform oscillating electric fields. Biophys J 74(2):1024–1030
86. Asbury CL, Diercks AH, van den Engh G (2002) Trapping of DNA by dielectrophoresis. Electrophoresis 23(16):2658–2666
87. Chou CF, Tegenfeldt JO, Bakajin O et al (2000) DNA trapping by electrodeless dielectrophoresis. APS March Meeting, Minneapolis, MN, USA
88. Chou C-F, Tegenfeldt JO, Bakajin O et al (2002) Electrodeless dielectrophoresis of single- and double-stranded DNA. Biophys J 83(4):2170–2179
89. Cummings EB, Singh AK (2000) Dielectrophoretic trapping without embedded electrodes. In: Mastrangelo CH, Becker H (eds) Microfluidic devices and systems III 4177:164–73
90. Ajdari A, Prost J (1991) Free-flow electrophoresis with trapping by a transverse inhomogenous field. Proc Natl Acad Sci USA 88:4468–4471
91. Washizu M, Kurosawa O (1990) Electrostatic manipulation of DNA in microfabricated structures. IEEE Trans Ind Appl 26(6):1165–1172
92. Washizu M, Kurosawa O, Arai I et al (1995) Applications of electrostatic stretch-and-positioning of DNA. IEEE Trans Ind Appl 31(3):447–455
93. Green NG, Morgan H, Milner JJ (1997) Dielectrophoresis of tobacco mosaic virus. Biophys J 72(2):MP448-MP
94. Morgan H, Green NG (1997) Dielectrophoretic manipulation of rod-shaped viral particles. J Electrostat 42(3):279–293
95. Hughes MP, Morgan H, Rixon FJ et al (1998) Manipulation of herpes simplex virus type 1 by dielectrophoresis. Biochim Biophys Acta 1425(1):119–126
96. Hughes MP, Morgan H, Rixon FJ (2001) Dielectrophoretic manipulation and characterization of herpes simplex virus-1 capsids. Eur Biophys J Biophys Lett 30(4):268–272
97. Green NG, Morgan H, Milner JJ (1997) Manipulation and trapping of sub-micron bioparticles using dielectrophoresis. J Biochem Biophys Methods 35(2):89–102

98. Archer S, Morgan H, Rixon FJ (1999) Electrorotation studies of baby hamster kidney fibroblasts infected with herpes simplex virus type 1. Biophys J 76(5):2833–2842
99. Krupke R, Hennrich F, von Löhneysen H et al (2003) Separation of metallic from semiconducting single-walled carbon nanotubes. Science 301:344–347
100. Svanvik N, Westman G, Wang D et al (2000) Light-up probes: thiazole orange-conjugated peptide nucleic acid for detection of target nucleic acid in homogeneous solution. Anal Biochem 281:26–35
101. Schwartz DC, Cantor CR (1984) Separation of yeast chromosome-sized DNAs by pulsed field gradient gel-electrophoresis. Cell 37(1):67–75
102. Kim Y, Morris MD (1995) Rapid pulsed field capillary electrophoretic separation of megabase nucleic acids. Anal Chem 67(5):784–786
103. Mitnik L, Heller C, Prost J et al (1995) Segregation of DNA solutions induced by electric fields. Science 267:219–222
104. Foquet M, Korlach J, Zipfel W et al (2002) DNA fragment sizing by single molecule detection in submicrometer-sized closed fluidic channels. Anal Chem 74(6):1415–1422
105. Chou HP, Spence C, Scherer A et al (1999) A microfabricated device for sizing and sorting DNA molecules. Proc Natl Acad Sci USA 96(1):11–13
106. Chu G, Vollrath D, Davis RW (1986) Separation of large DNA-molecules by contour-clamped homogeneous electric-fields. Science 234:1582–1585
107. Carle GF, Frank , Olson MV (1986) Electrophoretic separations of large DNA molecules by periodic inversion. Science 232:65–68
108. Han J, Turner SW, Craighead HG (1999) Entropic trapping and escape of long DNA molecules at submicron size constriction. Phys Rev Lett 83(8):1688–1691
109. Han J, Craighead HG (2000) Separation of long DNA molecules in a microfabricated entropic trap array. Science 288: 1026–1029
110. Han JY, Craighead HG (2002) Characterization and optimization of an entropic trap for DNA separation. Anal Chem 74(2):394–401
111. Turner SWP, Cabodi M, Craighead HG (2002) Confinement-induced entropic recoil of single DNA molecules in a nanofluidic structure. Phys Rev Lett 88(12): art no 128103
112. Duke TAJ, Austin RH, Cox EC et al (1996) Pulsed-field electrophoresis in microlithographic arrays. Electrophoresis 17(6): 1075–1079
113. Huang LR, Tegenfeldt JO, Kraeft JJ et al (2001) Generation of large-area tunable uniform electric fields in microfluid arrays for rapid DNA separation. Technical digest of the 2001 IEEE international electron devices meeting, pp 363–366
114. Astumian RD (1997) Thermodynamics and kinetics of a Brownian motor. Science 276:917–922
115. Astumian RD, Hanggi P (2002) Brownian motors. Phys Today 55(11):33–39
116. Chou CF, Bakajin O, Turner SWP et al (1999) Sorting by diffusion: an asymmetric obstacle course for continuous molecular separation. Proc Natl Acad Sci USA 96(24):13762–13765
117. van Oudenaarden A, Boxer SG (1999) Brownian ratchets: molecular separations in lipid bilayers supported on patterned arrays. Science 285:1046–1048
118. Duke TAJ, Austin RH (1998) Microfabricated sieve for the continuous sorting of macromolecules. Phys Rev Lett 80(7): 1552–1555
119. Ertas D (1998) Lateral separation of macromolecules and polyelectrolytes in microlithographic arrays. Phys Rev Lett 80(7):8–1551
120. Huang LR, Silberzan P, Tegenfeldt JO et al (2002) Role of molecular size in ratchet fractionation. Phys Rev Lett 89(17): art no 178301
121. Guo X-H, Huff EJ, Schwartz DC (1992) Sizing single DNA molecules. Nature 359:783–784
122. Cai W, Jing J, Irvin B et al (1998) High-resolution restriction maps of bacterial artificial chromosomes constructed by optical mapping. PNAS 95:3390–3395
123. Tegenfeldt JO, Bakajin O, Chou C-F et al (2001) Near-field scanner for moving molecules. Phys Rev Lett 86(7):1378–1381
124. Ohtsu M, Hori H (1999) Near-field nano-optics: from basic principles to nano-fabrication and nano-photonics. Kluwer Plenum, New York
125. Fillard JP (1997) Near field optics and nanoscopy. World Scientific, Singapore
126. Paesler MA, Moyer PJ (1996) Near-field optics: theory, instrumentation, and applications. Wiley
127. Thio T, Ghaemi HF, Lezec HJ et al (1999) Surface-plasmon-enhanced transmission through hole arrays in Cr films. J Opt Soc Am B 16(10):1743–1748
128. Chan WCW, Nie S (1998) Quantum dot bioconjugates for ultrasensitive nonisotopic detection. Science 281:2016–2018
129. Dubertret B, Skourides P, Norris DJ et al (2002) In vivo imaging of quantum dots encapsulated in phospholipid micelles. Science 298:1759–1762
130. Emory SR, Nie SM (1997) Near-field surface enhanced raman-spectroscopy on single silver nanoparticles. Anal Chem 69:2631
131. Nie SM, Emory SR (1997) Probing single molecules and single nanoparticles by surface-enhanced Raman-scattering. Science 275:1102
132. Emory SR, Haskins WE, Nie SM (1998) Direct observation of size-dependent optical enhancement in single metal nanoparticles. J Am Chem Soc 120:8009
133. Brochard-Wyart F (1995) Polymer-chains under strong flows – stems and flowers. Europhys Lett 30(7):387–392
134. Hagerman PJ (1988) Flexibility of DNA. Annu Rev Biophys Biophys Chem 17:265–286
135. Manning GS (1981) A procedure for extracting persistence lengths from light-scattering data on intermediate molecular-weight DNA. Biopolymers 20(8):1751–1755
136. Analysis performed on a Macintosh computer using the public domain NIH Image program (developed at the US National Institutes of Health and available on the Internet at http://rsb.info.nih.gov/nih-image/)
137. Yildiz A, Forkey JN, McKinney SA et al (2003) Myosin V walks hand-over-hand: single fluorophore imaging with 1.5-nm localization. Science 300:2061–2065
138. Thompson RE, Larson DR, Webb WW (2002) Precise nanometer localization analysis for individual fluorescent probes. Biophys J 82(5):2775–2783
139. Krylov SN, Arriaga E, Zhang ZR et al (2000) Single-cell analysis avoids sample processing bias. J Chromatogr B 741(1): 31–35